Rapid Fluctuations of the Subsurface Chlorophyll Maximum in Response to Wind Forcing in a Long, Narrow Bay

Esperanza Broullón[1], Peter J.S. Franks[2], Bieito Fernández Castro[3], Miguel Gilcoto[4], and Beatriz Mourino-Carballido[1]

[1]Universidade de Vigo
[2]Scripps Institution of Oceanography
[3]University of Southampton
[4]Instituto de Investigaciones Marinas- CSIC

August 28, 2021

Abstract

Bays within eastern boundary upwelling systems (EBUS) are ecological hot-spots featuring a diverse range of spatio-temporal dynamics. At the EBUSs' poleward limit, upwelling occurs in short-lived (<1 week) pulses modulated by synoptic wind variability. The circulations in long, narrow bays can respond to these fluctuations within few hours. The short-term biological response to these pulses was investigated in two of these bays (Rias Baixas, NW-Iberia) with a two-week quasi-synoptic spatio-temporal survey in the summer 2018. A four-day-long upwelling pulse caused deep, nutrient-rich isopycnals to rise into the euphotic zone inside the bays, triggering a rapid (~1.7 days) nutrient uptake and formation of a subsurface chlorophyll maximum (~3.8 days). The phytoplankton biomass was transported rapidly toward deep, offshore waters when the winds weakened. These results suggest that high productivity in narrow bays is controlled by the transient exposure of deep, nutrient-rich waters to light during upwelling pulses.

Rapid Fluctuations of the Subsurface Chlorophyll Maximum in Response to Wind Forcing in a Long, Narrow Bay

E. Broullón[1], P. J. S. Franks[2], B. Fernández Castro[3], M. Gilcoto[4]and B. Mouriño-Carballido[1]

[1]Departamento de Ecoloxía e Bioloxía Animal, Universidade de Vigo, Vigo, Spain
[2]Scripps Institution of Oceanography, University of California San Diego, La Jolla, CA, USA
[3]Ocean and Earth Science, National Oceanography Centre, University of Southampton, Southampton, UK
[4]Departamento de Oceanografía, Instituto de Investigacións Mariñas (IIM-CSIC), Vigo, Spain

Key Points:

- Upwelling events (∼3 days) in the Galician Rías Baixas are enhanced by the combination of shelf and local winds.
- Phytoplankton grow rapidly (1-3 days) within the upwelled nutrient-rich isopycnals when they are transiently exposed to light in the rías
- Short-lived phytoplankton blooms are controlled by the rapid, adiabatic and reversible upwelling of deep isopycnals.

Corresponding author: Esperanza Broullón, `ebroullon@gmail.com`, `esperanza.broullon.mandado@uvigo.es`

Abstract

Bays within eastern boundary upwelling systems (EBUS) are ecological hot-spots featuring a diverse range of spatio-temporal dynamics. At the EBUSs' poleward limit, upwelling occurs in short-lived (<1 week) pulses modulated by synoptic wind variability. The circulations in long, narrow bays can respond to these fluctuations within few hours. The short-term biological response to these pulses was investigated in two of these bays (Rías Baixas, NW-Iberia) with a two-week quasi-synoptic spatio-temporal survey in the summer 2018. A four-day-long upwelling pulse caused deep, nutrient-rich isopycnals to rise into the euphotic zone inside the bays, triggering a rapid (∼1.7 days) nutrient uptake and formation of a subsurface chlorophyll maximum (∼3.8 days). The phytoplankton biomass was transported rapidly toward deep, offshore waters when the winds weakened. These results suggest that high productivity in narrow bays is controlled by the transient exposure of deep, nutrient-rich waters to light during upwelling pulses.

Plain Language Summary

Equatorward winds off the main west continental coasts are responsible of the upwelling of deep, nutrient-rich waters to the surface. For this reason, eastern boundary upwelling systems (EBUS) are the most productive areas in the world's oceans. Bays within EBUS are ecological hot-spots that provide food and protection for a myriad of organisms. The circulation in long, narrow bays reacts very rapidly to short-lived upwelling pulses (∼3 days) related to weather patterns. In this study, we used high-resolution observations in two upwelling bays (Rías Baixas, NW Iberian Peninsula) to study how phytoplankton –the microalgae that sustain the ecosystem– respond to short-lived wind pulses. During a 17-day cruise, we documented a four-day-long southward upwelling-favorable wind event causing deep, nutrient-rich water to rise into the well-lit zone inside the bays. Phytoplankton rapidly uptook nutrients and grew within the upwelled waters, triggering the formation of an intense bloom. The bloom was then transported toward deep, offshore waters when the winds weakened. Our findings suggest that the extraordinary productivity of narrow, upwelling bays is underpinned by the rapid response of the plankton communities to the succession of intermittent short-lived upwelling events.

1 Introduction

Eastern boundary upwelling systems (EBUS) are among the most productive ocean ecosystems, supporting 10% of oceanic new production (Fréon et al., 2009), despite covering only $\sim 1\%$ of the global ocean's surface. The extraordinary biological productivity of these systems is driven by their hydrodynamics – in particular, their response to wind forcing. Equatorward winds drive Ekman transports that displace surface waters from the coast to the open ocean, resulting in the uplift of deep, nutrient-rich waters towards the euphotic zone. Bays located within EBUS can be even more productive than offshore waters, acting as hot-spots for phytoplankton growth. Due to their shape, bays can have long residence times of high-nutrient upwelled waters, providing retention zones with enhanced phytoplankton growth (Largier, 2020). These bays can thus support intense fishing and shellfish production through aquaculture (Trainer et al., 2010). Despite the common driving forces, EBUS are highly heterogeneous, presenting a diverse range of spatio-temporal dynamics depending on local bathymetry and the spatio-temporal variability of the wind forcing (Arístegui et al., 2009; Chavez & Messié, 2009). As localized upwelling hot-spots, bays within EBUS display a particularly rich suite of dynamical and ecosystem responses (Largier, 2020), which have profound implications for the communities relying on them as a source of food and services.

The Galician Rías Baixas are four long, narrow bays located at the northern limit of the Canary Current eastern boundary; here coastal upwelling supports a highly productive food chain and one of the most economically important marine industries in Europe (Blanton et al., 1987; Figueiras et al., 2002). Due to their latitudes, the temporal dynamics of upwelling in the rías are governed by synoptic-scale wind variability, which displays a strong seasonal modulation (Wooster et al., 1976). Southward, upwelling-favorable winds prevail between April and October, and northward downwelling-favorable winds from October to March (Wooster et al., 1976). As a consequence of fluctuating synoptic forcing, upwelling in these bays is not a steady process resulting from the large-scale equilibrium between the wind stress, the Coriolis force, and baroclinic pressure gradient, as in the classical formulations (Bowden, 1983). Instead, upwelling occurs as a series of transient events with a typical duration of $\sim$3.3 days, interspersed with relaxation or downwelling events (Gilcoto et al., 2017).

The circulation of the rías responds to changes in the wind forcing (Cordeiro et al., 2021) within $\sim$6 hours (Gilcoto et al., 2017). This is considerably faster than expected in a classical coastal upwelling system, where the shortest time scales relate to the rotational spin-up of the Ekman surface layer (Allen, 1973): the inertial period (17.85 hours at 42.23^{o} N). The fast response in the rías results from the combination of shelf and local winds, and the shape and dynamical characteristics of the rías. Local winds are funneled along the bays by the local topography, such that upwelling-favorable (respectively downwelling-favorable) winds over the shelf occur synchronously with down-bay (resp. up-bay) winds (Herrera et al., 2005; Gilcoto et al., 2017). Because the rías are relatively narrow and deep (deeper than the Ekman depth), the fast initial response to wind forcing occurs through an along-bay momentum balance involving the wind stress, the barotropic pressure gradient, and friction (note: not Coriolis) (Lentz & Fewings, 2012). This results in a rapid, linear spin-up of the exchange flow in response to upwelling/downwelling winds (see Supplementary Text 1). After the initial spin-up, the exchange flow is subsequently reinforced by the coupling of the slower rotational local (ría) and shelf responses (Souto et al., 2003; Barton et al., 2015; Gilcoto et al., 2017).

Recently, a combination of highly resolved observations in space (Barton et al., 2015) and time (Barton et al., 2016; Gilcoto et al., 2017; Fernández-Castro et al., 2018), with regional models (Souto et al., 2003; Cordeiro et al., 2021), has substantially increased our understanding of the hydrodynamical responses of the Rías Baixas to transient upwelling/downwelling pulses, however, due to a prior lack of fine-scale biochemical data, we do not have a detailed characterization of the ecosystem response to these dynamics in these rías. Thus, while plankton growth dynamics in the region are intrinsically linked to

high-frequency variability of the wind-driven circulation, they have been historically interpreted in terms of the seasonal variations of meteorological and environmental conditions (Nogueira et al., 1997; Nogueira & Figueiras, 2005; Díaz et al., 2016; Cermeño et al., 2006). Here we investigate the coupling between the high-frequency upwelling dynamics and plankton growth using data from a spatially extensive, temporally intensive survey around the two southern-most Rías Baixas (Ría de Vigo and Ría de Pontevedra) during the summer of 2018.

2 Materials and Methods

The REMEDIOS-TLP cruise was carried out between 29 June and 16 July 2018 in the northwest of the Iberian Peninsula, specifically in two long narrow bays (Ría de Pontevedra, north, and Ría de Vigo, south), and the adjacent shelf (Fig. 1c). The sampling area is located at the northern end of the Canary Current-Iberian Upwelling System where the regional circulation is affected by cycles of wind-driven upwelling and downwelling (Fraga, 1981). The mean water depth in the sampling domain ranged from 15 to 60 m between the inner and outer parts of the bays, dropping sharply at their mouth to ∼115 m deep at the westernmost sampling points over the shelf break (see Supplementary Figure S4).

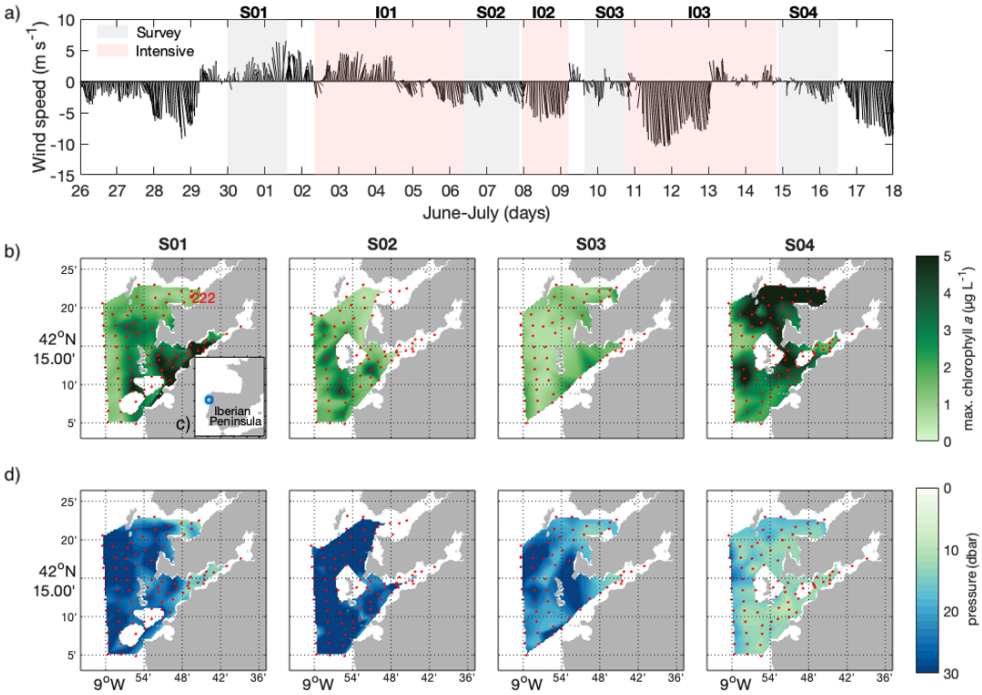

Figure 1. a) Time series of shelf winds throughout the cruise. Negative (positive) values correspond to upwelling (downwelling) favorable winds, mainly southward (northward) winds. Grey shaded areas show the survey sampling periods S01-S04, whereas the red areas indicate the intensive samplings I01-I03. b) Maximum chlorophyll *a* within the isopycnal range σ_t =26.4-27 $kg\ m^{-3}$. The first map shows the location of the intensive station, 222. c) Study area location within the Iberian Peninsula. d) Pressure at the maximum chlorophyll *a* concentration, within the same isopycnal range as b. Red dots in b and d correspond to the stations sampled in each survey.

A grid of 84 stations throughout the area (Fig. 1b) was sampled during four surveys on board of R/V Ramón Margalef: S01 (29 June to 01 July), S02 (6-7 July), S03 (9-10 July) and S04 (14-16 July). The survey samplings were interspersed by three periods of intensive sampling at a fixed station inside the Ría de Pontevedra (station 222, ∼30 m, 42.35°N, 8.77°W): I01 (02-06 July), I02 (07-09 July) and I03 (10-14 July).

During the survey samplings (S01-S04), a SBE911 conductivity-temperature-depth (CTD) profile was acquired at each station. The SBE911 was equipped with fluorescence and photosynthetically active radiation (PAR)t sensors.

During the intensive samplings (I01-I03), CTD profiles were recorded with a MSS90 microstructure profiler (Prandke & Stips, 1998) equipped among others with a fluorescence sensor. Five casts were performed every half hour, gathering a total of 1675 profiles over the three intensive samplings. These continuous measurements were paused every six hours (8 am, 2 pm, 8 pm, 2 am) to conduct water collection at 7-8 depths with a rosette equipped with 12 Niskin bottles, for determination of inorganic nutrients and chlorophyll concentrations. These chlorophyll samples, as well as other samples collected during the seasonal samplings of the REMEDIOS project (March 2017 to May 2018) were used to calibrate the MSS90 fluorescence sensor ($n = 65$). The fitted calibration curve was:

$$chlorophyll\,a = 1.460 \times fluorescence - 0.248,\ (R^2 = 0.901) \tag{1}$$

To calibrate the fluorescence sensor of the SBE911, a set of chlorophyll samples collected during the cruise at different stations throughout the study area was used ($n = 71$):

$$chlorophyll\,a = 0.270 \times fluorescence - 0.051,\ (R^2 = 0.855) \tag{2}$$

To determine nitrate concentrations, samples were frozen *in situ* at -18°C and analysed on land with a Skalar San Plus segmented flux analyser.

Wind data spanning the REMEDIOS-TLP period were acquired from an oceanographic buoy at the shelf (42.12°N, 9.43°W) operated by Puertos del Estado (data available at www.puertos.es); whereas wind data near the intensive station were acquired from the meteorological station located at Cabo Udra, Bueu (42.34°N, 8.82°W) operated by Meteogalicia (data available at meteogalicia.gal).

3 Results

Time series of shelf wind (Fig. 1a) showed a strong upwelling-favorable wind event before the cruise, which relaxed a few hours before the initial spatial survey (S01). The following days were characterized mainly by northward, downwelling-favorable winds until the middle of the first occupation of the intensive time-series station (I01), on 4 July. Subsequently, southward, upwelling-favorable winds increased to a maximum on 11-13 July, during I03. This increase was interrupted by two days of weak winds coinciding with S03, on 9-10 July. Finally, the last 3-4 days of the cruise, coinciding with S04, were dominated by upwelling relaxation.

The subsurface chlorophyll maximum tended to follow isopycnals, and was located between $\sigma_\theta = 26.4 - 27$ kg m^{-3} during the study (Fig. 1b and 1d). During the field campaign, these isopycnals fluctuated up and down, and in and out of the rías depending on the upwelling-relaxation-downwelling state. The first 3-day sampling survey, S01, was conducted a day after an upwelling event, and during a downwelling event. High maximum chlorophyll values of ($2.6 \pm 1.9\,\mu$g L^{-1}) were detected over the whole area (Fig. 1b). In Ría de Vigo and over the shelf, the chlorophyll concentrations were greater than $5\,\mu$g L^{-1} at several stations. The mean depth of the isopycnal range containing the chlorophyll maximum was 26 ± 8 m, deeper than the mean euphotic depth in the rías (10% incident light, mean depth 16 ± 2 m), and deeper over the shelf and the mouth of the rías (>20 m) than in their interior (∼18 m). During S02, two days after a downwelling event, the chlorophyll maximum was weaker ($1.5 \pm 1.0\,\mu$g L^{-1}), and deeper than during the S01 survey (32 ± 9 m). Moreover, the isopycnal range was not present in the inner part of the rías, presumably an effect of the wind-driven downwelling. The subsurface chlorophyll maximum was weakest during S03

($1.2 \pm 0.6\,\mu g\,L^{-1}$), but it was shoaling ($23 \pm 7$ m in the rías) following upwelling-favorable conditions during the preceding days. By survey S04, the deep chlorophyll maximum was located much shallower than during previous surveys (15 ± 4 m in the rías), and had reached its highest concentrations ($3.3 \pm 1.8\,\mu g\,L^{-1}$).

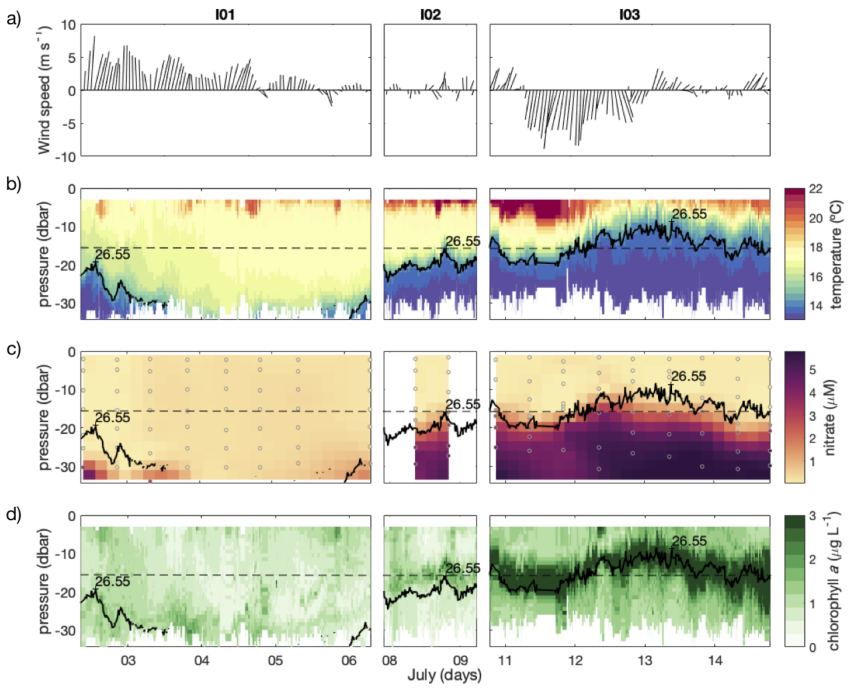

Figure 2. Time-series of a) wind, b) temperature, c) nitrate, and d) chlorophyll *a* during the occupations of the intensive station inside Ría de Pontevedra, 222. Black solid lines in panels b, c, and d represent the 26.4 kg m^{-3} isopycnal. Black dashed lines in panels b, c, and d represent the mean 10% incident light at intensive station, 222. Dots in panel c indicate when bottle samples were taken. In order to improve the representation, maximum of chlorophyll values was set to 3 $\mu g\,L^{-1}$, thus values above 3 $\mu g\,L^{-1}$ are not distinguished in panel d.

The intensive sampling time series at a single station in the ría, I01-I03, offer a higher-resolution temporal view of the chlorophyll dynamics inside the rías in response to variability in the wind forcing (Fig. 2b-d). In particular, large vertical fluctuations of the isopycnals containing the chlorophyll maximum are apparent at this station; these isopycnals showed at least a 25 m vertical excursion (close to the full depth range), closely coupled with the various upwelling-downwelling cycles. With the onset of downwelling-favorable winds at the beginning of I01, the chlorophyll-rich isopycnals (centered at 26.55 kg m^{-3}) deepened (29 ± 3 m), and showed only weak chlorophyll-maximum values ($1.0 \pm 0.3\,\mu g\,L^{-1}$). Toward the end of I01, winds shifted to weakly upwelling-favorable and the 26.55 kg m^{-3} isopycnal shoaled (Fig. 2b). Nitrate levels were very low, exceeding 1 μM only below the chlorophyll maximum when those isopycnals were present (Fig. 2b-d). The next intensive sampling, I02, occurred after several days of weakly upwelling-favorable winds. During I02, the isopycnals containing the chlorophyll maximum shoaled, raising the chlorophyll maximum up to 20 ± 2 m depth; maximum chlorophyll values were still low ($0.8 \pm 0.3\,\mu g\,L^{-1}$). During I03, after two days of relaxation when the nutrient-rich isopycnals deepened slightly, a period of sustained, intense upwelling caused the isopycnals to rapidly shoal further to < 10 m, well within the euphotic zone. The shoaling isopyncals were accompanied by the upward movement of nutrient-rich water into the base of the euphotic zone. During this time the chlorophyll values increased to their highest values during the study ($> 5\,\mu g\,L^{-1}$).

4 Discussion

The different samplings developed during the cruise can be re-sorted in time (Fig. 3) to illustrate the response of the deep chlorophyll maximum to a typical wind-driven upwelling cycle. Before the intensification of southward, upwelling-favorable winds, (as encountered during I01 and S02), nutrient-rich isopycnals contain low chlorophyll and are found deep ($>$ 30 m) in waters over the shelf; they are not present in the shallow ($<$ 25 m) middle-inner part of the bays. When the wind starts blowing from the north (upwelling favorable), a circulation develops inside the bays driving the surface layer offshore, causing the deep isopycnals to rapidly shoal in the inner part of the rías. This shoaling brings deep, nutrient-rich water up to the base of the euphotic zone, allowing an increase of subsurface chlorophyll concentrations there, as in I02 and S03. During this upwelling in the rías, the isopycnals are still deep at the mouth of the ría, and over the shelf. If the upwelling-favorable wind continues, the nutrient-rich isopycnals are also advected upward into the euphotic zone over the shelf. At this point the bloom is in its most intense and widespread phase, with highest chlorophyll values found inside the bays where the isopycnals are shallower (e.g., I03 and S04). Finally, the wind relaxes or reverses to downwelling-favorable, causing the dense, chlorophyll-containing isopycnals to deepen and flow back offshore from the rías. As the chlorophyll-maximum layer deepens below the euphotic zone, the chlorophyll concentrations decrease, as found during S01.

The intensive sampling I03 showcases the rapid biological response to wind-driven fluctuations of isopycnals. At the beginning of this sampling, at 6 pm on 10 July, chlorophyll levels were high, but relatively deep ($\sim$ 17 m) due to the preceding upwelling/relaxation conditions (Fig. 3d). Upwelling-favorable winds started blowing at 4 am, on 11 July. Almost synchronously, the chlorophyll maximum layer reverted its deepening trend and began to shoal until 5 pm on 12 July. The layer remained stable above 10 m for 21 hours (Fig. 3c). The shoaling of the 26.55 kg m^{-3} isopycnal was immediately followed by a reduction of the nitrate concentrations (Fig. 2c, 3b) and an increase in chlorophyll concentrations (Fig. 2d, 3c). This is consistent with the phytoplankton on these nutrient-rich isopycnals being exposed to light, and responding by rapidly taking up nutrients, with subsequent accumulation of biomass. This enhanced phytoplankton growth is locally restricted to the deep, nutrient-rich waters when they are exposed to light. The isolation of these isopycnals from the surface shows that diapycnal mixing of nutrients into surface waters – a much slower process than upward advection of isopycnals – plays a secondary role in the rapid development of the bloom.

The time scales of the phytoplankton response during I03 can be computed as the e-folding times of nitrate uptake ($\tau_{NO_3^-}$ = 1.74 d, Fig. 4a) and chlorophyll accumulation (τ_p = 3.80 d, Fig. 4b) in the isopyncal range of the chlorophyll maximum. The wind decorrelation time scale of 3.2 d, computed for the complete upwelling season of 2018 (Fig. 4c), represents the duration of a typical upwelling event (Gilcoto et al., 2017). The biological time scales are thus comparable to or shorter than the duration of an upwelling cycle, allowing the biomass of phytoplankton to show an exponential increase over the course of an upwelling cycle.

Our observations thus show that phytoplankton can respond rapidly to the transient exposure of deep, nutrient-rich isopycnals to light, resulting in significant nutrient uptake and subsequent bloom formation, in spite of the short duration of wind-driven upwelling pulses ($\sim$ 3 days). The coupling between the time scales of wind forcing and phytoplankton growth could therefore explain the high phytoplankton primary productivity of the rías in the region (Arístegui et al., 2009). Further, the succession of synoptic-scale upwelling events ensures that high average primary productivity is maintained throughout the summer season despite the flushing of biomass offshore after the cessation of upwelling-favorable winds.

This bio-physical coupling is intensified by the rapid response of the isopycnal depths in the rías to changes in wind forcing – much faster than the Ekman spin-up time. The long

and narrow (< baroclinic Rossby radius of deformation) morphometry of the rías (Largier, 2020) means that the Coriolis force plays a secondary role in setting up the circulation patterns. Instead, the initial spin-up of the ría's circulation is a non-rotational response to the local – rather than shelf – winds (Gilcoto et al., 2017) (see also Supplementary Text 1). Furthermore, the mountains surrounding the bays channel the remote and mostly meridional winds in the along-bay direction, driving the surface water layer downwind (Gilcoto et al., 2017) to create rapid upwelling and downwelling in the rías.

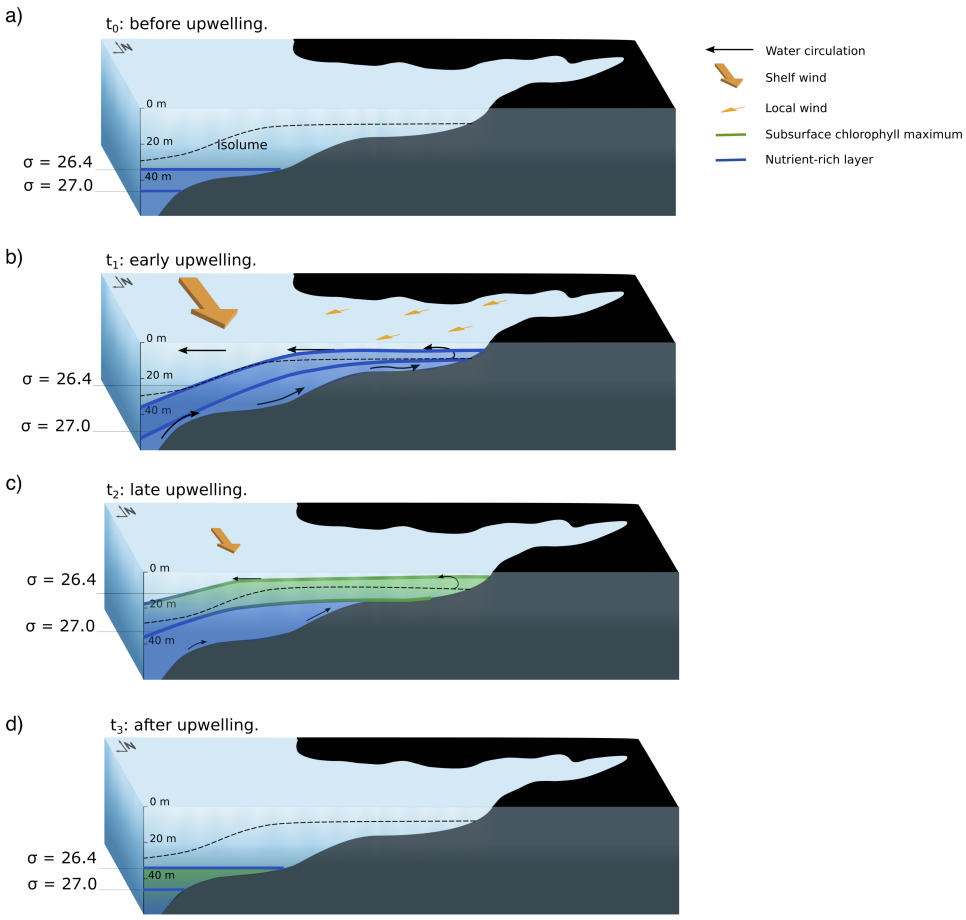

Figure 3. 3D schematics of a wind-driven upwelling cycle. a) Before upwelling: nutrient-rich isopycnals ($\sigma_t = 26.4 - 27\ kg\ m^{-3}$) are deep (I01 and S02). b) Early upwelling: wind stress forces surface waters down the bay. As a consequence, the isopycnals shoal into the euphotic zone inside the bays (I02 and S03). c) Late upwelling: high chlorophyll biomass forms when the nutrient-rich isopycnals are exposed to the light in the whole area (I03 and S04). d) After upwelling: as wind stops or reverses, the isopycnals deepen, carrying the high phytoplankton biomass with it (S01).

These rapid, wind-driven fluctuations of the pycnocline may also occur in other wind-forced bays that share the morphometric characteristics of the Galician rías. For example, Concepción bay (Chile), located in the Humboldt EBUS, is also classified as an elongated bay (Largier, 2020) and is oriented in the direction of the wind field during upwelling (northward winds), but partially sheltered from upwelling transport due to its south-to-north alignment. Though we do not have data from Concepción Bay, Daneri et al. (2012) and Peterson et al. (1988) studied Coliumo Bay, which is smaller, but adjacent to Concepción bay, and with a similar orientation. Transient upwelling events driven by synoptic wind forcing modulate the high primary productivity of this area (Daneri et al., 2012). Both studies (Daneri et al., 2012; Peterson et al., 1988) showed a lag time between wind stress and hydrographic

fluctuations of about 1 day, which is consistent with the local inertial period ($\sim$ 20 h). However, owing to their daily sampling interval, it is not possible to know whether more rapid hydrographic fluctuations were occurring; we would predict changes on an hourly time scale due to the similarity of this bay to our system.

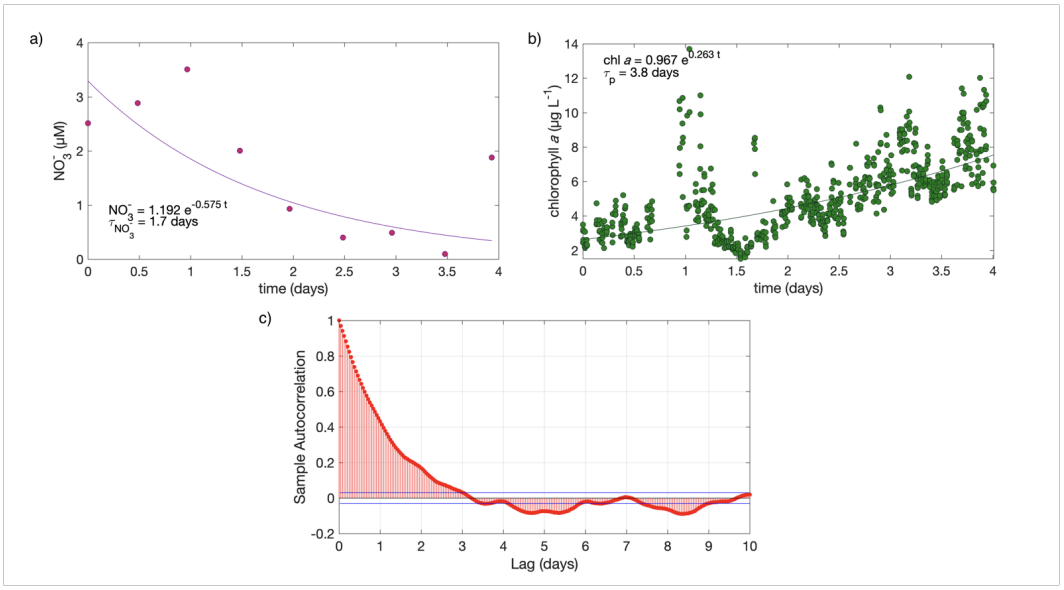

Figure 4. Exponential fits of a) nitrate and b) chlorophyll vs. time at $\sigma_\theta = 26.55$ kg m^{-3} during I03. Fitted equations and e-folding times for chlorophyll (τ_p) and nitrate ($\tau_{NO_3^-}$) are shown. c) 10 days of the autocorrelation function and 95% confidence intervals (blue lines) for along-shore wind from the full 2018 upwelling season time series (15 April to 15 October).

Another elongated bay, Dakhla Bay, located in the Canary Current EBUS (Largier, 2020) is one of the most productive areas in Morocco in terms of shellfish farming (Zidane et al., 2008). It is also oriented NE to SW, as our bays, and the typical winds in the region are mainly from north and north-east (Zidane et al., 2008; Van Camp et al., 1991). This bay fits all the requirements to have rapid fluctuations of the subsurface chlorophyll maximum in response to both local and shelf wind forcing. However, no high-temporal-resolution samplings have been carried out here so far.

Our results have implications for mussel farming – the most productive marine aquaculturing activity in the region (Labarta & Fernández-Reiriz, 2019). Mussels are cultured on 12-m long ropes hanging from rafts. The intermittent presence of nutrient-rich water near the surface is likely to affect mussel food supply and growth. Local mussel farmers report that the growth of mussels located near the surface is twice the growth of mussels deeper down on the ropes. However, they also point out that the deepest end of the rope (10 to 12 m) often has much larger mussels as well. These deep mussels are likely accessing the subsurface nutrient-rich, high-phytoplankton-biomass layer observed during upwelling conditions in our cruise. It is possible that longer ropes – with more frequent access to this layer – could benefit the mussel culture.

Every year, mussel harvesting is threatened by the presence of harmful algae blooms. Often, these harmful blooms appear related to the presence of thin chlorophyll layers (Broullón et al., 2020). However, traditional monitoring programs using either oceanographic bottle samples taken at specific depth intervals or vertically integrated hose samples (Escalera et al., 2012; McManus et al., 2008; Velo-Suárez et al., 2008) may not adequately sample such layers. The dynamics of thin layer formation and their connections to harmful blooms remain poorly understood in this region, which hampers our ability to predict their occurrence, or offer useful advice to mussel farmers. In contrast, the high-resolution chlorophyll observations reported here showed the development of a subsurface chlorophyll

maximum which, at least during part of intensive sampling I03, had the characteristics of a thin layer (< 3 m thick). This finding underscores the need for highly spatially and temporally resolved observations to better understand the biophysical processes involved in thin layer formation and their connections to harmful blooms.

5 Conclusions

The aim of this study was to investigate the coupling between phytoplankton growth and upwelling dynamics in two long, narrow bays (Ría de Vigo and Ría de Pontevedra, NW Spain) using a highly temporally and spatially resolved dataset collected during the 3-week REMEDIOS-TLP cruise (July 2018). Our results show that the long, narrow bay led to a rapid response of the along-bay circulation to along-bay winds – much faster than the inertial response found offshore. Short ($\sim$ 3 day) upwelling-favorable wind events caused isopycnals to rapidly shoal in the bay, exposing deep, nutrient-rich isopycnals to light. Phytoplankton on these deep isopycnals quickly ($\sim$ 2 days) took up nutrients, and increased in biomass ($\sim$ 3 days). This enhanced phytoplankton biomass fluctuated with wind-driven fluctuations of the isopycnal depths, and was advected into and out of the bays depending on the wind stress. Our data show that such short-lived phytoplankton blooms in these bays are controlled by the rapid, adiabatic and reversible upwelling of deep isopycnals, rather than the fertilization of surface waters by diapycnal turbulent mixing. It is therefore likely that these short-time-scale blooms explain the overall elevated biological productivity of such bays. Similar bio-physical coupling dynamics may drive high primary productivity in other upwelling bays that have comparable morphologies and orientations; these dynamics will only be revealed through highly spatially and temporally resolved surveys, such as those presented in this study.

Acknowledgments

The authors would like to thank the captain, crew, and technicians of R/V Ramón Margalef as well as Nicolás Villacieros, Fernando Alonso and Waldo Redondo from IIM-CSIC and Paloma Chouciño from Universidade de Vigo for their help in processing data from land during the REMEDIOS-TLP cruise and in the preparation of the equipment before. This research was funded by project REMEDIOS (CTM2016-75451-C2-1-R) to B. M-C from the Spanish Ministry of Economy and Competitiveness. E. B. acknowledges a predoctoral fellowship (ED481A-2019/288) from Xunta de Galicia, co-funded by FSE Galicia (2014-2020). B. F. C. is supported by the European Union's Horizon 2020 research and innovation program under the Marie Skłodowska-Curie grant agreement No. 834330 (SO-CUP). Bathymetry data used in the Supplementary Information was obtained from GEBCO Compilation Group (2020) GEBCO 2020 Grid (https://doi.org/10.5285/a29c5465-b138-234d-e053-6c86abc040b9). Data sets for used in this research are available in Mendeley Data reposistory at http://dx.doi.org/10.17632/pm4r2pyyh3.1.

References

Allen, J. S. (1973). Upwelling and Coastal Jets in a Continuously Stratified Ocean. *Journal of Physical Oceanography*, *3*(3). doi: 10.1175/1520-0485(1973)003⟨0245:uacjia⟩2.0.co;2

Arístegui, J., Barton, E. D., Álvarez-Salgado, X. A., Santos, A. M. P., Figueiras, F. G., Kifani, S., ... Demarcq, H. (2009). Sub-regional ecosystem variability in the Canary Current upwelling. *Progress in Oceanography*, *83*(1-4), 33–48. doi: 10.1016/j.pocean.2009.07.031

Barton, E., Largier, J., Torres, R., Sheridan, M., Trasviña, A., Souza, A., ... Valle-Levinson, A. (2015). Coastal upwelling and downwelling forcing of circulation in a semi-enclosed bay: Ria de Vigo. *Progress in Oceanography*, *134*, 173–189. doi: 10.1016/J.POCEAN.2015.01.014

Barton, E., Torres, R., Figueiras, F. G., Gilcoto, M., Largier, J., Gil-Coto, M., & Largier, J. (2016). Surface water subduction during a downwelling event in a semienclosed bay. *Journal of Geophysical Research: Oceans*, *121*(9), 7088–7107. doi: 10.1002/2016JC011950

Blanton, J. O., Tenore, K. R., Castillejo, F., Atkinson, L. P., Schwing, F. B., & Lavin, A. (1987). The relationship of upwelling to mussel production in the rias on the western coast of Spain. *Journal of Marine Research*, *45*(2), 497–511. doi: 10.1357/002224087788401115

Bowden, K. F. (1983). Physical oceanography of coastal waters. In (Ellis Horw ed.). Chichester. doi: https://doi.org/10.1016/0377-0265(85)90006-5

Broullón, E., López-Mozos, M., Reguera, B., Chouciño, P., Doval, M. D., Fernández-Castro, B., ... Mouriño-Carballido, B. (2020). Thin layers of phytoplankton and harmful algae events in a coastal upwelling system. *Progress in Oceanography*, *189*, 102449. doi: 10.1016/J.POCEAN.2020.102449

Cermeño, P., Marañón, E., Pérez, V., Serret, P., Fernández, E., & Castro, C. G. (2006). Phytoplankton size structure and primary production in a highly dynamic coastal ecosystem (Ría de Vigo, NW-Spain): Seasonal and short-time scale variability. *Estuarine, Coastal and Shelf Science*, *67*(1-2), 251–266. doi: 10.1016/j.ecss.2005.11.027

Chavez, F. P., & Messié, M. (2009). A comparison of Eastern Boundary Upwelling Ecosystems. *Progress in Oceanography*, *83*(1-4), 80–96. doi: 10.1016/J.POCEAN.2009.07.032

Cordeiro, N. G., Nolasco, R., Barton, E. D., & Dubert, J. (2021). Fixed-point time series, repeat survey and high-resolution modeling reveal event scale responses of the Northwestern Iberian upwelling. *Progress in Oceanography*, *190*, 102480. doi: 10.1016/J.POCEAN.2020.102480

Daneri, G., Lizárraga, L., Montero, P., González, H. E., & Tapia, F. J. (2012). Wind forcing and short-term variability of phytoplankton and heterotrophic bacterioplankton in the coastal zone of the Concepción upwelling system (Central Chile). *Progress in Oceanography*, *92-95*, 92–96. doi: 10.1016/J.POCEAN.2011.07.013

Díaz, P. A., Ruiz-Villarreal, M., Pazos, Y., Moita, T., & Reguera, B. (2016). Climate variability and *Dinophysis acuta* blooms in an upwelling system. *Harmful Algae*, *53*, 145–159. doi: 10.1016/j.hal.2015.11.007

Escalera, L., Pazos, Y., Dolores Doval, M., & Reguera, B. (2012). A comparison of integrated and discrete depth sampling for monitoring toxic species of *Dinophysis*. *Marine Pollution Bulletin*, *64*(1), 106–113. doi: 10.1016/j.marpolbul.2011.10.015

Fernández-Castro, B., Gilcoto, M., Naveira-Garabato, A. C., Villamaña, M., Graña, R., & Mouriño-Carballido, B. (2018). Modulation of the Semidiurnal Cycle of Turbulent Dissipation by Wind-Driven Upwelling in a Coastal Embayment. *Journal of Geophysical Research: Oceans*, *123*(6), 4034–4054. doi: 10.1002/2017JC013582

Figueiras, F. G., Labarta, U., & Reiriz, M. J. F. (2002). Coastal upwelling, primary production and mussel growth in the Rías Baixas of Galicia. In *Sustainable increase of marine harvesting: Fundamental mechanisms and new concepts* (pp. 121–131). Dordrecht: Springer Netherlands. doi: 10.1007/978-94-017-3190-4_11

Fraga, F. (1981). Upwelling off the Galician coast, Northwest Spain. *Coastal and Estuarine Sciences: Coastal Upwelling*, *1*, 176–182. doi: 10.1029/co001p0176

Fréon, P., Barange, M., & Arístegui, J. (2009). Eastern Boundary Upwelling Ecosystems: Integrative and comparative approaches. *Progress in Oceanography*, *83*(1-4), 1–14. doi: 10.1016/j.pocean.2009.08.001

Gilcoto, M., Largier, J. L., Barton, E. D., Piedracoba, S., Torres, R., Graña, R., ... Granda, F. (2017). Rapid response to coastal upwelling in a semienclosed bay. *Geophysical Research Letters*, *44*(5), 2388–2397. doi: 10.1002/2016GL072416

Herrera, J. L., Piedracoba, S., Varela, R. A., & Rosón, G. (2005). Spatial analysis of the wind field on the western coast of Galicia (NW Spain) from in situ measurements. *Continental Shelf Research*, *25*, 1728–1748. doi: doi:10.1016/j.csr.2005.06.001

Labarta, U., & Fernández-Reiriz, M. J. (2019). The Galician mussel industry: Innovation

and changes in the last forty years. *Ocean and Coastal Management*, *167*, 208–218. doi: 10.1016/j.ocecoaman.2018.10.012

Largier, J. L. (2020). Upwelling Bays: How Coastal Upwelling Controls Circulation, Habitat, and Productivity in Bays. *Annual Review of Marine Science*, *12*(1), 415–447. doi: 10.1146/annurev-marine-010419-011020

Lentz, S. J., & Fewings, M. R. (2012). The wind -and wave- driven inner-shelf circulation. *Annual Review of Marine Science*, *4*, 317–343. doi: 10.1146/annurev-marine-120709-142745

McManus, M. A., Kudela, R. M., Silver, M. W., Steward, G. F., Donaghay, P. L., & Sullivan, J. M. (2008). Cryptic blooms: Are thin layers the missing connection? *Estuaries and Coasts*, *31*(2), 396–401. doi: 10.1007/s12237-007-9025-4

Nogueira, E., & Figueiras, F. G. (2005). The microplankton succession in the Ría de Vigo revisited: Species assemblages and the role of weather-induced, hydrodynamic variability. In *Journal of marine systems* (Vol. 54, pp. 139–155). doi: 10.1016/j.jmarsys.2004.07.009

Nogueira, E., Pérez, F. F., & Ríos, A. F. (1997). Seasonal patterns and long-term trends in an estuarine upwelling ecosystem (Ria de Vigo, NW Spain). *Estuarine, Coastal and Shelf Science*, *44*(3), 285–300. doi: 10.1006/ecss.1996.0119

Peterson, W. T., Arcos, D. F., McManus, G. B., Dam, H., Bellantoni, D., Johnson, T., & Tiselius, P. (1988). The nearshore zone during coastal upwelling: Daily variability and coupling between primary and secondary production off central Chile. *Progress in Oceanography*, *20*(1), 1–40. doi: 10.1016/0079-6611(88)90052-3

Prandke, H., & Stips, A. (1998). Test measurements with an operational microstructure-turbulence profiler: Detection limit of dissipation rates. *Aquatic Sciences*, *60*(3), 191. doi: 10.1007/s000270050036

Souto, C., Gilcoto, M., Farina-Busto, L., & Pérez, F. F. (2003). Modeling the residual circulation of a coastal embayment affected by wind-driven upwelling: Circulation of the Ría de Vigo (NW Spain). *Journal of Geophysical Research: Oceans*, *108*(11). doi: 10.1029/2002jc001512

Trainer, V. L., Pitcher, G. C., Reguera, B., & Smayda, T. J. (2010). The distribution and impacts of harmful algal bloom species in eastern boundary upwelling systems. *Progress in Oceanography*, *85*(1-2), 33–52. doi: 10.1016/j.pocean.2010.02.003

Van Camp, L., Nykjaer, L., Mittelstaedt, E., & Schlittenhardt, P. (1991). Upwelling and boundary circulation off Northwest Africa as depicted by infrared and visible satellite observations. *Progress in Oceanography*, *26*(4), 357–402. doi: 10.1016/0079-6611(91)90012-B

Velo-Suárez, L., González-Gil, S., Gentien, P., Lunven, M., Bechemin, C., Fernand, L., ... Reguera, B. (2008). Thin layers of *Pseudo-nitzschia spp.* and the fate of *Dinophysis acuminata* during an upwelling-downwelling cycle in a Galician Ría. *Limnology and Oceanography*, *53*(5), 1816–1834.

Wooster, W. S., Bakun, A., & McLain, D. R. (1976). The seasonal upwelling cycle along the eastern boundary of the North Atlantic. *Journal of Marine Research*, *34*, 131–141.

Zidane, H., Orbi, A., Mouradi, A., Zidane, F., & Blais, J. (2008). Structure hydrologique et edaphique d'un site ostreicole: duna Blanca (La baie de Dakhla Sud du Maroc). *Environmental Technology*, *29*(9), 1031–1042. doi: 10.1080/09593330802180328

Supporting Information for "Rapid Fluctuations of the Subsurface Chlorophyll Maximum in Response to Wind Forcing in a Long, Narrow Bay"

E. Broullón[1], P. J. S. Franks[2], B. Fernández Castro[3], M. Gilcoto[4]and B. Mouriño-Carballido[1]

[1]Departamento de Ecoloxía e Bioloxía Animal, Universidade de Vigo, Vigo, Spain

[2]Scripps Institution of Oceanography, University of California San Diego, La Jolla, CA, USA

[3]Ocean and Earth Science, National Oceanography Centre, University of Southampton, Southampton, UK

[4]Departamento de Oceanografía, Instituto de Investigacións Mariñas (IIM-CSIC), Vigo, Spain

Contents of this file

1. Text S1

2. Figures S1 to S4

Dynamical equations for the barotropic response of the Ría

Let's take the Ría as a rectangular channel extending in the x direction (the y direction is assumed to be irrelevant, as we neglect rotation) with a length L and a height h at equilibrium, and study the barotropic response to an along-channel wind stress (τ_w). At the west end of the Ría, the height is fixed (we assume that the volume of the adjacent

ocean is infinite), and at the inner eastern end the surface position can vary. We define the surface height anomaly with respect to the equilibrium as η (Fig. S1).

The response is determined by the continuity equation and the momentum equation in the x axis. We reduce the problem to two dimensions by resolving the eastward velocity, $u(z,t)$, of the Ría at its mouth ($x = 0$). The continuity equation:

$$\frac{\partial u}{\partial x} + \frac{\partial v}{\partial y} + \frac{\partial w}{\partial z} = 0 \tag{1}$$

is reduced to two dimensions and written in an integral form:

$$\int_0^h \frac{\partial u}{\partial x} dz + \frac{\partial \overline{\eta}}{\partial t} = h\frac{\partial \overline{u}}{\partial x} + \frac{\partial \overline{\eta}}{\partial t} = 0 \tag{2}$$

where $\overline{\eta}$ is the mean height within the Ría, which corresponds to half of the height in the eastern-most point, $\overline{\eta} = \eta/2$. Because the eastward velocity is zero at the solid wall ($x = L$):

$$\frac{\partial \overline{u}}{\partial x} = \frac{\overline{u}(x=L) - \overline{u}(x=0)}{L} = -\frac{\overline{u}(x=0)}{L} \equiv -\frac{\overline{u}}{L} \tag{3}$$

So then we have as continuity equation:

$$\boxed{\frac{\partial \eta}{\partial t} = 2h\frac{\overline{u}}{L}} \tag{4}$$

On the other hand, the momentum equation in the x direction:

$$\frac{Du}{Dt} = fv - \frac{1}{\rho}\left(\frac{\partial p}{\partial x} + \frac{\partial \tau_x}{\partial z}\right) \tag{5}$$

We neglect the non linear terms ($\frac{Du}{Dt} \approx \frac{\partial u}{\partial t}$), and also Coriolis acceleration ($fv \approx 0$), and we follow a hydrostatic approximation ($p = g\rho(z+\eta)$). Because at $x = 0$, $\eta = 0$, for every z:

$$\frac{\partial p}{\partial x} = \frac{p(x=L) - p(x=0)}{L} = \frac{g\rho\eta}{L} \tag{6}$$

We model the shear stresses with a turbulent viscosity (κ):

$$\tau_x(z,t) = -\rho\kappa\frac{\partial u}{\partial z}(z,t) \tag{7}$$

With all this, the momentum equation is reduced to:

$$\boxed{\frac{\partial u}{\partial t} = -\frac{g\eta}{L} + \kappa\frac{\partial^2 u}{\partial z^2}} \tag{8}$$

with boundary conditions:

$$u(z=0) = 0 \tag{9}$$

and

$$\rho\kappa\frac{\partial u}{\partial z}(z=h) = \tau_w \tag{10}$$

where we calculated

$$\tau_w = \rho_{air} C_D W^2 \tag{11}$$

To illustrate this non-rotational barotropic response of the Ría to an along-channel wind pulse we performed a simulation using equations 4, and 8 to 11, by taking $h = 40$ m, $L = 30$ km, $g = 9.81$ m s^{-2}, $\rho_a = 1.2$ kg m^{-3}, $\rho = 1000$ kg m^{-3}, $C_D = 10^{-3}$ and $\kappa = 5 \times 10^{-4}$ m^2 s^{-1}. The wind was set to $W = -10$ m s^{-1} (offshore) between days 2 and 5 of the simulation. A 30 day spin off was used to allow the system to equilibrate and damp oscillations. Figure S2 shows the result of the simulation. As soon as the wind starts blowing, the water level inside the Ría drops by ~ 20 cm and starts oscillating at relatively high frequency (< 1 h). At the same time a bidirectional flow, with outflowing surface layer and inflowing bottom layer starts to develop immediately, first with strong linear acceleration, and equilibrates slowly (due to the action of viscosity) over the duration of

the wind pulse (3 days, a typical value for the system). However, full equilibrium seems not to be reached.

There are two inherent time-scales to this response. First, the barotropic along-Ría time-scale which determines the propagation of the pressure perturbation signal along the channel, and an equilibration time-scale which depends on the damping effect of viscosity. The barotropic time scale can be determined by neglecting the viscous term in Eq. 8 (second term on the right hand side), and by derivating and substituting with Eq. 4, taking into account that for a barotropic response without friction or wind forcing the velocity profile is uniform, $u(z) = \overline{u}$:

$$\frac{\partial^2 u}{\partial t^2} = -\frac{g}{L}\frac{\partial \eta}{\partial t} \Rightarrow \frac{\partial^2 u}{\partial t^2} = -\frac{2hg}{L2}u \tag{12}$$

This is the equation for an harmonic oscillation with frequency $\omega = (\frac{2hg}{L^2})^{1/2}$. Hence, the barotropic period is:

$$T_{bt} = 2\pi\omega^{-1} \approx 1.90\,\mathrm{h} \tag{13}$$

So the barotropic response of the Ría starts to develop in less than a couple of hours. This is also the frequency of the oscillations observed in the water level. However, the acceleration time-scale (and the equilibrium exchange velocities) are dictated by the equilibrium between the pressure gradient and the frictional response. The equilibrium solution could be find analytically by taking $\frac{\partial u}{\partial t}, \frac{\partial \eta}{\partial t} = 0$ in Eq. 4 and 8. Because we are interested on the dynamic response (equilibration time), we performed instead three simulations with different values of κ and for a wind pulse extending between days 2 and 10 of the simulation, in order to allow some extra time for equilibration (Fig. S3). This figure shows that the equilibrium exchange velocities are larger for weaker viscosities. Viscosity

values of $5 - 10 \times 10^{-4}$ m^2 s^{-1} produced realistic equilibrium exchange velocities (10-20 cm s^{-1}) (Barton et al., 2015), but those were unrealistically high for a weaker viscosity of $\kappa = 0.1 \times 10^{-4}$ m^2 s^{-1}. This figure also illustrates the linear response of the Ría until the viscosity effects become important. Until a time scale t for which $u = u_{max}/2$, the response is almost linear. This time scale was of about half a day (smaller than the local inertial period of 0.75 days) for $\kappa = 10\times^{-4}$ m^2 s^{-1}, and of about 1 day for $\kappa = 5 \times 10^{-4}$ m^2 s^{-1}. In any case, the bidirectional circulation is set-up almost immediately, while a rotational response would need to wait one inertial period or more such that the along-shore circulation equilibrates with the Coriolis force.

References

Barton, E., Largier, J., Torres, R., Sheridan, M., Trasviña, A., Souza, A., ... Valle-Levinson, A. (2015). Coastal upwelling and downwelling forcing of circulation in a semi-enclosed bay: Ria de Vigo. *Progress in Oceanography*, *134*, 173–189. doi: 10.1016/J.POCEAN.2015.01.014

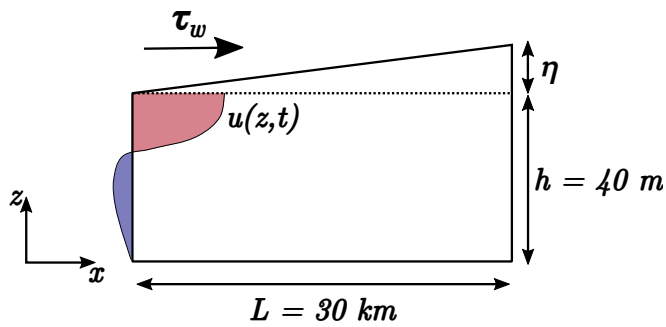

Figure S1. Schematics of the dynamical balance of barotropic response of the Ría to an along-channel wind stress (τ_w).

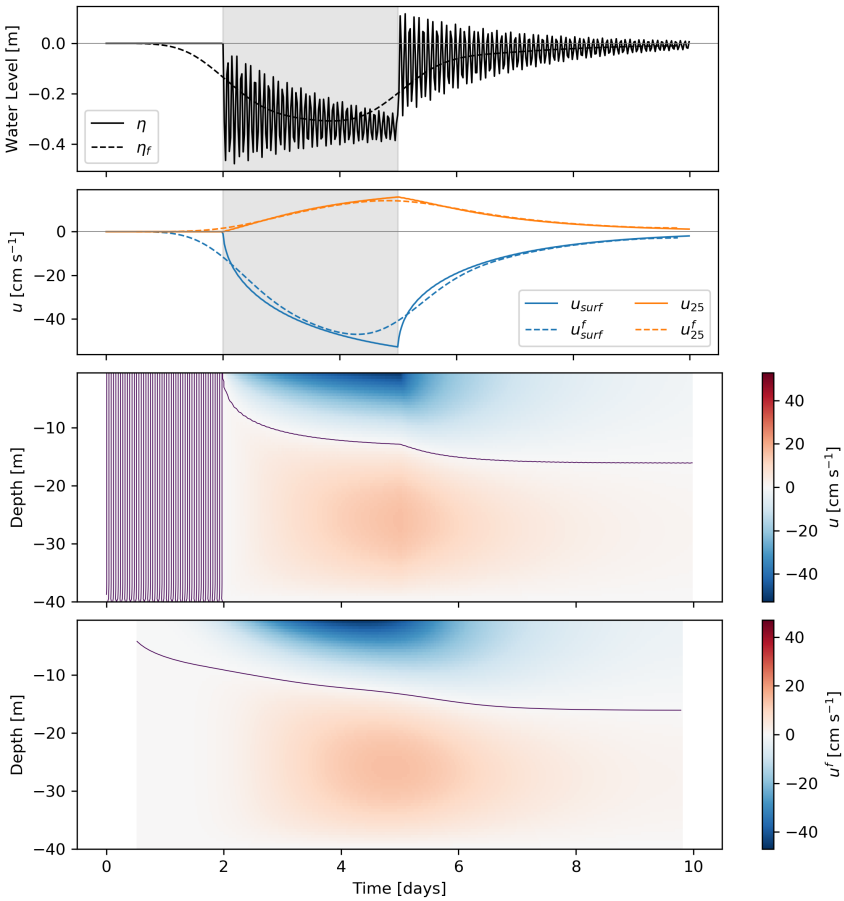

Figure S2. Simulation of the Ría response to a down-channel wind pulse of $W = 10$ m s^{-1} during days 2-5 of the simulation using the barotropic model. Water level at the inner-most point (η) and eastward velocities (u) are shown. The f index indicates quantities filtered with a Godin 24/25/24 filter. In the second panel, the velocity at the surface layer ($z = 0.5$ m) and at 25 m depth are displayed. In this simulation, the turbulent viscosity is set to $\kappa = 5 \times 10^{-4}$ m^2 s^{-1}.

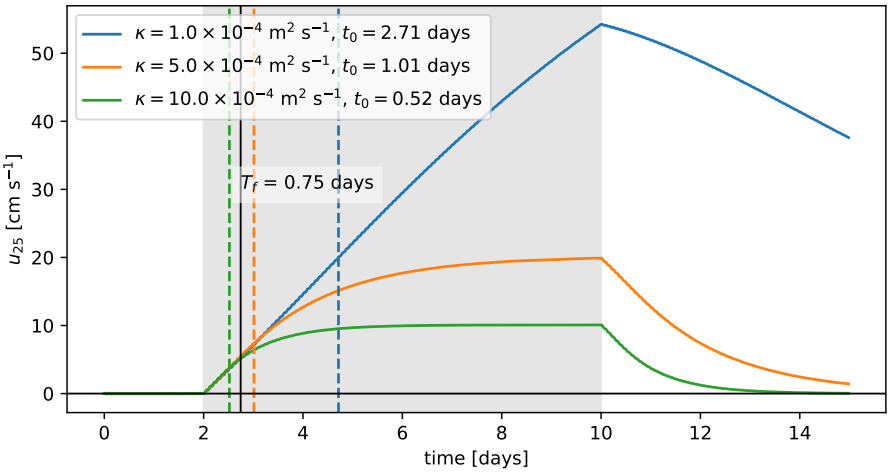

Figure S3. Along-channel velocities at 25 m depth for simulations of the barotropic non-rotational response of the Ría to a wind pulse $W = -10$ m s^{-1} between days 2 and 12 of the simulation, with different values of the turbulent viscosity coefficient (κ). The response time (t_0) is the time required for u to reach $1/e$ of its maximum value. The inertial period T_f is shown for comparison.

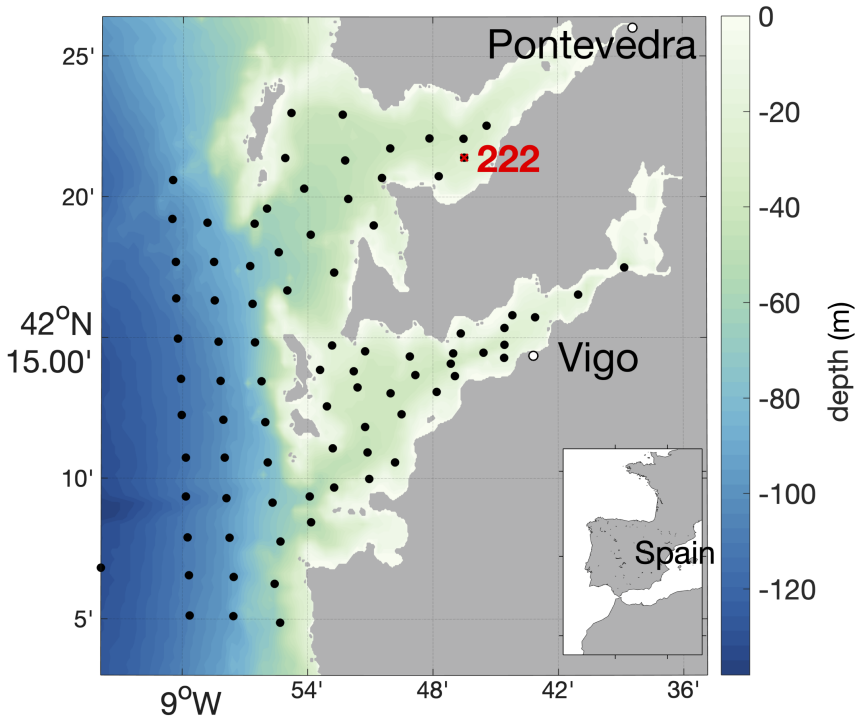

Figure S4. Bathymetry map of the two southernmost Galician Rías Baixas: Ría de Pontevedra and Ría de Vigo. Black dots indicate the sampling stations during REMEDIOS-TLP cruise. The red cross indicates the intensive sampling station, 222. Bathymetry data ta from GEBCO Compilation Group (2020) GEBCO 2020 Grid (doi:10.5285/a29c5465-b138-234d- e053-6c86abc040b9).